Journal of Physics:
Conference Series

PURPOSE-LED
PUBLISHING™

PAPER • **OPEN ACCESS**

GH3536 superalloy prepared by selective laser melting: microstructure and properties

To cite this article: Y Zhang *et al* 2023 *J. Phys.: Conf. Ser.* **2639** 012015

View the article online for updates and enhancements.

You may also like

- Influence of laser power and scan speed on the microstructure and properties of GH4169 alloy prepared by selective laser melting
Jianguo Chen, Xuanbo Wang and Yingcai Pan
- Study on microstructure and mechanical properties of 4Cr5MoSiV1 steel manufactured by selective laser melting
Yanchao Bi, Fenghe Tao, Changzhi Jia et al.
- Effect of Hot Isostatic Pressing on Microstructure and Properties of GH4169 Superalloy Manufactured by SLM
Zhoujin Lv, Shuo Chen, Lida Che et al.

Enabling Electrochemistry
Inside and Outside the Lab

PalmSens

Discover our diverse range of Potentiostats engineered to support your research wherever it takes you

- Intuitive software for Windows and Android
- Proven in over 4000 scientific publications
- Single-channel and multi-channel
- Benchtop, portable and wearable

Discover More



This content was downloaded from IP address 158.69.200.216 on 07/11/2026 at 16:23

GH3536 superalloy prepared by selective laser melting: microstructure and properties

Y Zhang[1,2], Y Wang[2], B Zhang[1], M Song[2], Y Li[2] and Y Li[2]

[1] Postdoctoral Station of Materials Science and Engineering, Harbin Engineering University, Harbin, 150000, P.R.China

[2] Institute of Advanced Technology, Heilongjiang Academy of Sciences, Harbin, 150000, P.R.China
Email: smh1980@126.com

Abstract. In this paper, GH3536 superalloy was prepared by selective laser melting (SLM) using plasma rotating electrode powder as raw material. The effects of forming and heat treatment processes on the microstructure and mechanical properties of GH3536 superalloy were studied. The results show that there were obvious micro-cracks on the laser scanning plane of SLM samples, and the length of micro-cracks was between 10-100μm. The micro-cracks originated from the inside of the molten pools and penetrated the melting channels, and the heat treatment could not eliminate the cracks. With the in-crease of volume energy density (VED), the tensile strength and yield strength of SLM samples increased first and then decreased. The maximum values of tensile strength and yield strength reached 772.3MPa and 613.3MPa, respectively. However, with the increase of VED, the elongation of SLM samples decreased to 27.3%. After heat treatment, the tensile strength and yield strength of the material increased (up to 789MPa and 410MPa), but the elongation decreased.

1. Introduction

GH3536 is a typical nickel-based superalloy with good oxidation resistance, corrosion resistance, hot and cold working formability and weldability. It has broad application prospects in aviation, aerospace and engine fields [1]. In recent years, with the design of GH3536 alloy components more complex, higher performance and accuracy requirements, the traditional casting, forging and powder metallurgy processes are difficult to meet the above requirements [2].

Selective Laser Melting (SLM) is an additive manufacturing technology that uses laser to selectively melt the metal powder layer by layer according to the three-dimensional slice model of the part, and finally realizes the die-less, fully dense and near net shape forming of complex metal components [3]. Compared with the traditional manufacturing process, SLM has the advantages of high forming precision, good surface quality and complex shape parts. At the same time, it can effectively reduce the number of weld beads and parts in traditional manufacturing, so as to achieve high reliability, intensification and lightweight, especially suitable for precision and rapid manufacturing of complex structural parts [4-6]. At present, the research of SLM preparing metal components mainly focuses on titanium alloy, stainless steel and Inconel718, etc. There are relatively few reports on the preparation of GH3536 superalloy. At the same time, only density, microstructure and mechanical properties of GH3536 superalloy are briefly analysed, and the mechanism is not studied in depth.

In addition, powder is undoubtedly the key factor, which affects GH3536 alloy parts prepared by SLM. At present, the reported GH3536 alloys prepared by SLM are all made of powders prepared by gas atomization. This method has the advantages of wide particle size distribution, high sphericity, low impurity content and low cost, but there are many problems, such as satellite powders and hollow powders [7]. The presence of hollow powder will increase the impurity content in the powder, which are mainly rare gases in the milling process. These rare gas impurities cannot form a solid solution or

Content from this work may be used under the terms of the Creative Commons Attribution 3.0 licence. Any further distribution of this work must maintain attribution to the author(s) and the title of the work, journal citation and DOI.
Published under licence by IOP Publishing Ltd

compound with GH3536 alloy, and will remain to form pores during rapid melting and solidification, thereby reducing the mechanical properties of the formed parts [8]. Therefore, improving powder properties and optimizing SLM process parameters is the key to regulating the microstructure of GH3536 superalloy. The plasma rotating electrode process has the advantages of high powder sphericity, good surface morphology, low impurity content, and the powder particle size distribution can be adjusted by rotating speed and electrode diameter [9]. The use of plasma as a heat source greatly reduces the impurities in the preparation of the powders. At the same time, because there is no impact of high-pressure gas and the influence of gas circulation, there is basically no hollow powder and satellite powder. However, there is no report on GH3536 superalloy prepared by SLM using powders of plasma rotating electrode process.

Therefore, in this paper, GH3536 superalloy samples were prepared by SLM using powders of plasma rotating electrode process as raw material. The effects of SLM preparing and heat treatment process on the microstructure and mechanical properties of GH3536 superalloy were studied, which provided theoretical basis and practical reference for additive manufacturing of GH3536 superalloy.

2. Experimental procedure

2.1. Experimental material

In this experiment, self-made GH3536 superalloy powder was used, and its preparation process was plasma rotating electrode+thermal plasma spheroidization. The composition of GH3536 alloy powder was shown in Table 1.The microstructure of the powder was observed by Hitachi S4700SEM, as shown in Figure 1.

It can be seen from Figure1(a) and (b) that the powder morphology is mostly spherical or nearly spherical, which can obtain better fluidity. The Easizer30 laser particle size analyser was used to detect the size of the powder. The particle diameter distribution is shown in Figure 1(c). The average particle size is 44.63pm. The size of the powder shows a normal distribution. This powder is conducive to flow and improves the density of the powder. The morphology and specifications of the particles were analysed by optical transmission microscopy. A total of 500g of powders were randomly selected, and the images were captured using the Olympus CX31 (bright field mode) Infinity1-5 fast imaging system. Image scope M was used to process the images. The results are shown in Figure 1(d), and there is no impurity in GH3536 superalloy powders.

In this paper, 0.45% carbon steel is selected as the substrate material, and the size of the substrate is 250mm×250mm×35mm. The substrate is derusted and deoiled, and polished by a grinder until the entire substrate surface presents a metallic luster and is relatively flat. Clean the substrate with acetone before use and dry it with a hairdryer.

Table 1. Chemical constituents of GH3536 superalloy (wt.%).

C	Mn	Si	S	P	Cu	Fe
0.05-0.15	1.0	1.0	0.015	0.025	0.5	17.0-20.0
W	Cr	Ni	Al	Ti	Co	Mo
0.2-1.0	20.5-23.0	Bal	0.5	0.15	0.5-2.5	8.1-10.0

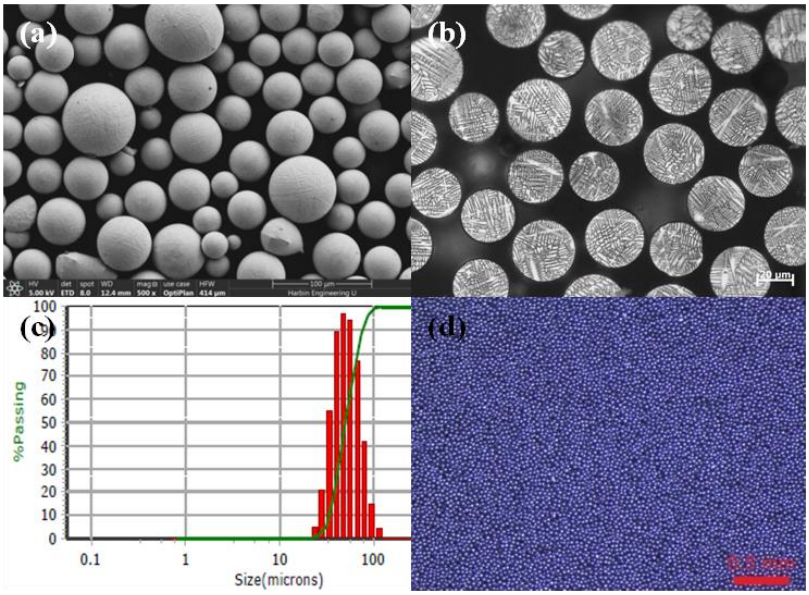


Figure 1. Self-made GH3536 powder: (a) powder macroscopic morphology; (b) Powder cross-sectional morphology; (c) Powder particle size distribution; (d) Powder impurities illustration of tensile samples.

2.2. SLM process parameters

This experiment used FS271M 3D printer (Huashu High Tech Company, China). Before printing, argon gas is introduced to exhaust the air until the oxygen content drops to 0.2%, forming a protective atmosphere. During printing, it is preheated to 100℃.

Adopting optimized forming process parameters: laser power 260W, scanning spacing 0.1mm, layer thickness 0.03mm. The scanning method is a chessboard to minimize stress, and then the sample is wire cut. The laser power P, scanning rate V, and scanning line spacing H have important effects on SLM. In fact, the quality of the formed part depends on the combined effect of the above parameters. In order to study the combined effect of the above parameters, the concept of volume energy density (VED) is used. The calculation formula for VED is as follows:

$$\mathrm{VED} = \frac{\mathrm{P}}{v \times h \times d} \times 10^{6} \quad (1)$$

P- Laser power, W; υ- Scanning rate, mm/s; h - Powder thickness, μm; d - Scan line spacing, μm.

The parameters were combined according to the L9 orthogonal experimental table. During the forming process, the powder thickness was fixed at 40 μm. The forming process parameters and VED are show n in Table 2.

Table 2. Process parameters

Sample number	P（W）	V（mm/s）	H（μm）	VED（J/mm^3）
1	250	800	0.03	104.2
2	250	900	0.03	92.6
3	250	1000	0.03	83.3
4	260	800	0.03	108.3
5	260	900	0.03	96.3
6	260	1000	0.03	86.7
7	270	800	0.03	112.5
8	270	900	0.03	100
9	270	1000	0.03	90

2.3. Heat treatment process

According to the characteristics of the alloy, two heat treatment systems were developed, namely aging heat treatment and solid solution+aging heat treatment. Two groups of SLM samples were selected for heat treatment. The OTF-1200 X vacuum tube furnace produced by Hefei Kejing Material Technology Co., Ltd, China, was used for heat treatment, and the heating rate was 10°C/min. The specific process is shown in Table 3.

Table 3. Heat treatment process of GH3536 alloy

Heat treatment process	Process
Aging (HT1)	720℃/8h+620℃/8h /furnace cooling
Solid solution+aging (HT2)	980℃/1h / water cooling +720℃/8h +620℃/8h/ furnace cooling

2.4. Microstructure and properties characterization

The Carl Zeiss-AxioVert.A1 metallographic microscope (OM), FEI-Sirion scanning electron microscope (SEM) and JEM-2100 transmission electron microscope (TEM) were used to observe the microstructure of the samples. The tensile test was carried out by WDW-100 microcomputer controlled electronic universal testing machine, and the sample size was shown in Figure2. The density and hardness of the samples were measured by SOPTOP AE124 density measuring instrument and HBRV-187.5 Brouwer hardness tester, respectively.

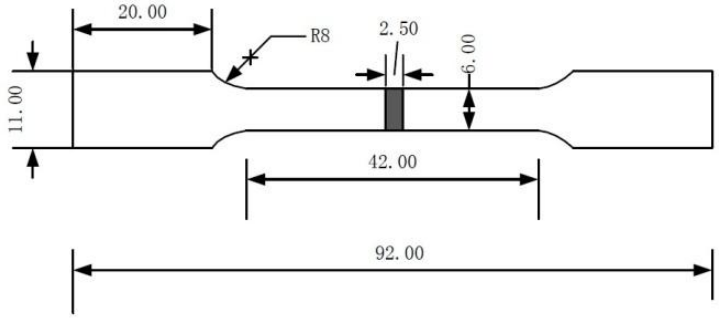


Figure 2. Schematic illustration of tensile samples.

3. Results and discussion

3.1. Microstructure observation of SLM samples

3.1.1 Metallographic structure observation.

The microstructure of GH3536 superalloy prepared by SLM after corrosion is shown in Figure3. From the figures, it can be seen that there are significant differences in the microstructure and crack morphology of the samples in the horizontal and vertical directions.It can be seen from Figure.3(a) that there are obvious intersecting strip molten pools on the laser scanning plane, and the melting channels are continuously distributed. There are micro-cracks on the surface of the sample, and the crack length is between 10~100μm, which is mainly distributed in the interior of the molten pools (as shown in Figure.3 (c)). By analysing the high-magnification microstructure of the micro-cracks (Figure.3e), it can be seen that the cracks mainly originate from the grain boundary. This is because the grain growth direction in this area is inconsistent, and the solidification shrinkage produces tensile stress in different directions on the unsolidified metal liquid, resulting in the tearing of the liquid film and the formation of solidification hot cracks. Figure.3 (b) is the microstructure along the forming direction. The boundary of the molten pools is scaly distributed, and the adjacent molten pools overlap well. The high-magnification microstructure along the laser scanning direction in Figure.3 (d) shows that the interior of the molten pools are columnar crystals growing perpendicular to the boundary of the molten pool in the direction of inverse temperature gradient. High magnification microstructure (Figure.3 (f)) can be observed perpendicular to the boundary of the molten pools to the centre of the mol-ten pools convergence growth of small columnar crystals, intergranular spacing between 0.8~1.5μm. The unique molten pool structure of SLM samples is unfavourable to mechanical

properties. Under the action of shear stress, cracks are easy to germinate and expand in the middle of the molten pool, which greatly reduces the plasticity of the material.

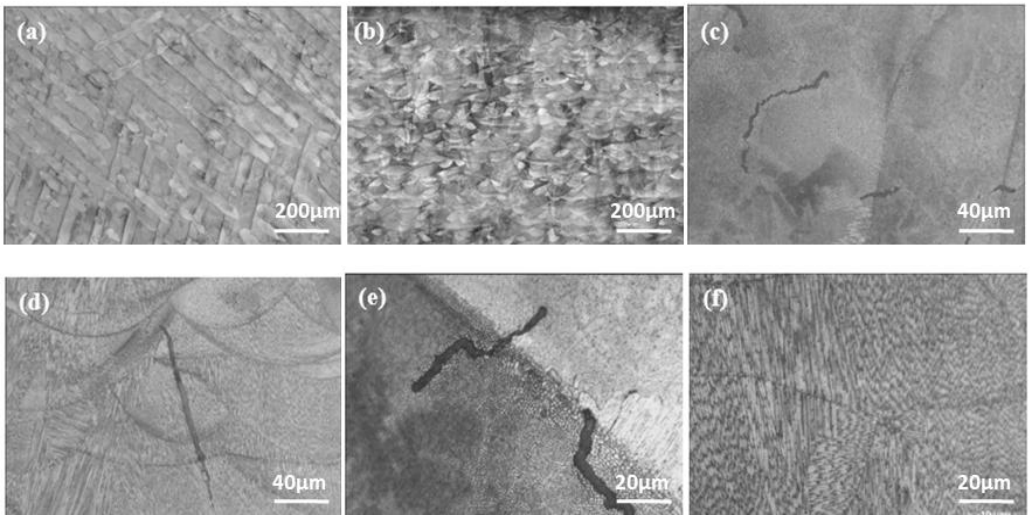


Figure 3. Microstructure of GH3536 superalloy prepared by SLM: (a) (c) (e) Horizontal direction; (b) (d) (f) Vertical direction.

3.1.2 Observation of pores and micro-cracks.

Figure 4 shows the polished morphology of the longitudinal section of SLM samples. It can be seen from the figure that as VED increases, the pores of the material gradually decrease, while the number of micro-cracks gradually increases. When VED is 86.3J/mm^3~96.3J/mm^3, there are pores formed in the unmelted area between the scanning lines inside the sample, and as VED increases, the internal pores gradually decrease and disappear. When VED is 96.3J/mm^3~112.5J/mm^3, micro-cracks begin to appear inside the sample, and the number of micro-cracks increases with the in-crease of VED. When VED is 112.5J/mm^3, there is no hole in the sample, and the number of micro-cracks is the largest.

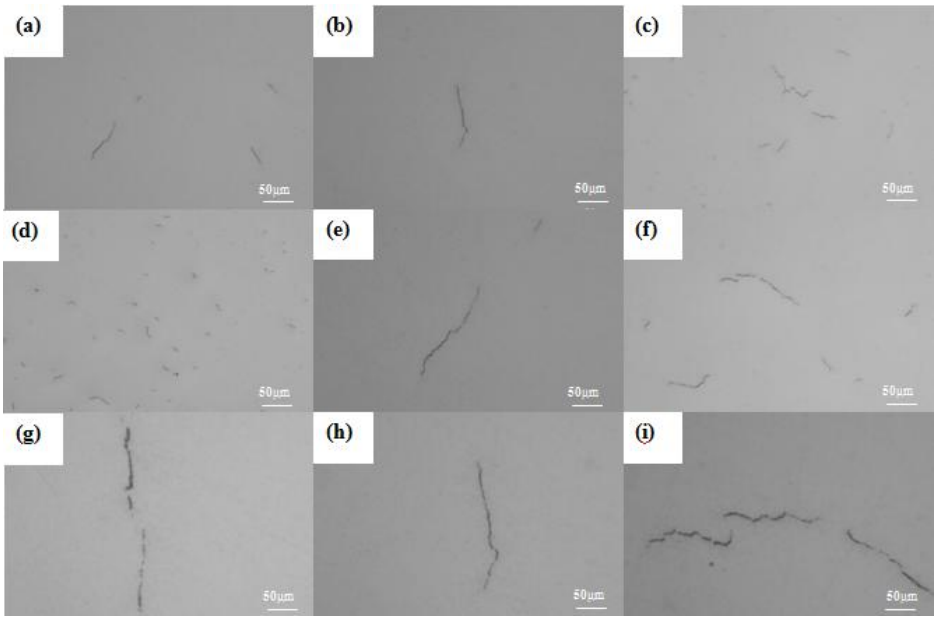


Figure 4. The change of cross-section morphology of GH3536 samples with different VED: (a) VED=83.3J/mm^3; (b) VED=86.7J/mm^3; (c) VED=90J/mm^3; (d) VED=92.6J/mm^3; (e) VED=96.3J/mm^3; (f) VED=100J/mm^3; (g) VED=104.2J/mm^3; (h)VED=108.3J/mm^3; (i) VED=112.5J/mm^3

3.1.3 Distribution of alloy elements.

Figure 5 shows the element distribution of GH3536 superalloy prepared by SLM. It can be seen from Figure 5 that there is segregation of C, Cr, Mo and other elements in the microstructure of SLM samples. The segregation of Cr and Mo elements increases the tendency of precipitation of Laves phase in the structure, thereby increasing the tendency of forming micro-cracks.

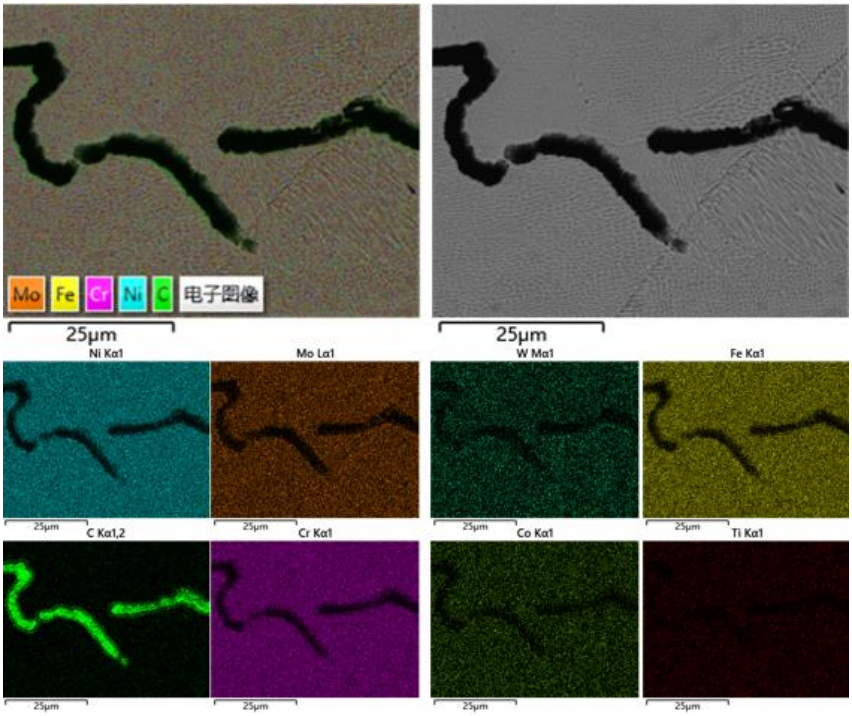


Figure 5. The distribution of alloying elements in GH3536 samples prepared by SLM

3.2. Eeffect of heat treatment on microstructure

3.2.1Effect of heat treatment on microstructure of GH3536 samples.

Figure6 is a comparison of the metallographic structure of SLM samples and that after heat treatment. From Figure6 (a) and (b), it can be seen that there are obvious ' layer-to-layer ' and ' channel-to-channel ' weld pool boundaries in SLM samples. After aging treatment, the overlapping zones of the molten pool boundary become shallow (as shown in Figure6 (c) and (d)). After solution + aging treatment, the molten pool boundary basically disappears (as shown in Figure6 (e) and (f)). The molten pool boundary is one of the factors that cause the anisotropy of mechanical properties of GH3536 superalloy. Therefore, heat treatment can reduce the anisotropy of GH3536 alloy, and the disappearance of molten pool boundary can improve the mechanical properties to a certain extent. In addition, it can be found from the figure that there are micro-cracks in the microstructure of GH3536 alloy samples before and after heat treatment, which indicates that heat treatment cannot eliminate micro-cracks. The micro-crack is the key factor restricting the plasticity of the material. Since the heat treatment fails to improve the micro-cracks in the GH3536 sample, its plasticity cannot be significantly improved.

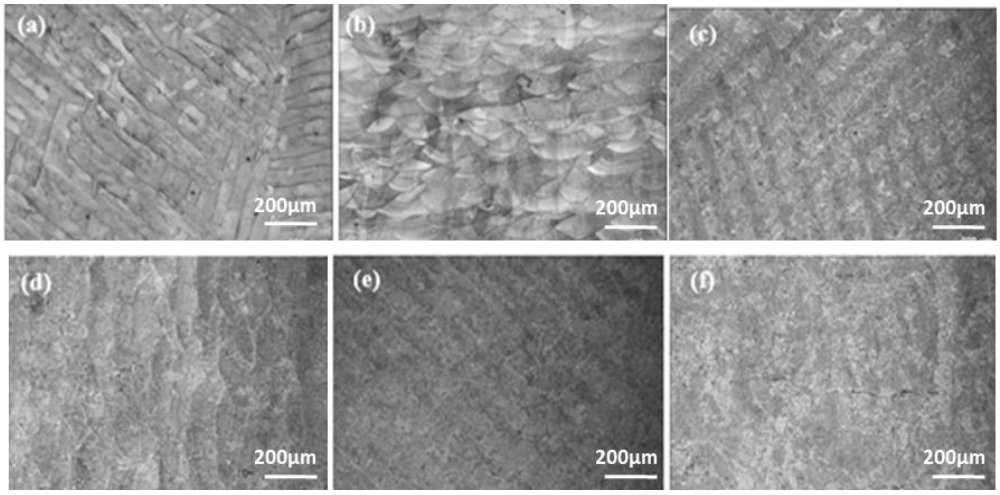


Figure 6. The effect of heat treatment on the microstructure of GH3536: (a) horizontal direction of SLM; (b) vertical direction of SLM; (c) horizontal direction of HT1; (d) vertical direction of HT1; (e) horizontal direction of HT2; (f) vertical direction of HT2.

3.2.2 Observation of microstructure of GH3536 samples through TEM.

It is known that GH3536 is a nickel-based solid solution strengthening superalloy. The microstructure at room temperature is mainly austenite. After SLMand heat treatment, $M_{23}C_6$, M_6C and σ phases will be precipitated [10]. The TEM analysis of the nano-scale structure of the solid solution+aging samples is shown in Figure7. It can be seen from Figure 7 (b) that after solution+aging heat treatment, the content of C, Cr and Mo at the grain boundary increased significantly, and Ni decreased significantly. The segregation of these elements promoted the precipitation of carbides and Laves phases. The EDS analysis of the precipitated phase (as shown in Figure 7 (d)) shows that the mass fraction ratio of Cr and Mo elements in the needle rod-like and lamellar phase regions at the grain boundary is close to 1: 1, and the phase composition is Cr_2Mo. According to the elemental composition of the common precipitated phase of GH3536 alloy, it can be determined as Laves phase. The needle bar (lamellar) Laves phase is often the location of micro-crack nucleation and propagation, which significantly reduces the plasticity and rupture strength of the superalloy. In order to improve the mechanical properties of GH3536, the precipitation of Laves phase is controlled by high temperature solution treatment.

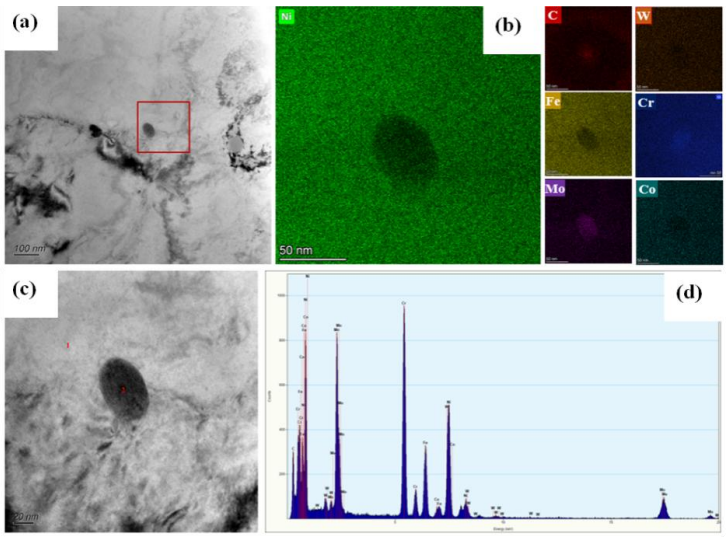


Figure 7. TEM photos of GH3536 alloy samples after heat treatment.

3.3. The effect of SLM process on the properties of GH3536 alloy

3.3.1 Effect of VED on the number of micro-cracks.

Figure8 shows the variation curve of the number of micro-cracks in the SLM samples with VED. On the whole, as VED increases, the number of micro-cracks in the sample gradually increases, which is consistent with the results observed in Figure 4. When VED is low, the input energy of the powder bed is low, and there is a large amount of unmelted metal powder, which forms pores after the powder falls off. With the increase of VED, the unmelted powder decreases and the pores decrease until they disappear. At the same time, with the increase of VED, the temperature of the metal molten pool increases, the temperature gradient increases, and the thermal expansion and contraction in different regions and their inhomogeneity increase, resulting in the increase of micro-cracks with the increase of VED.

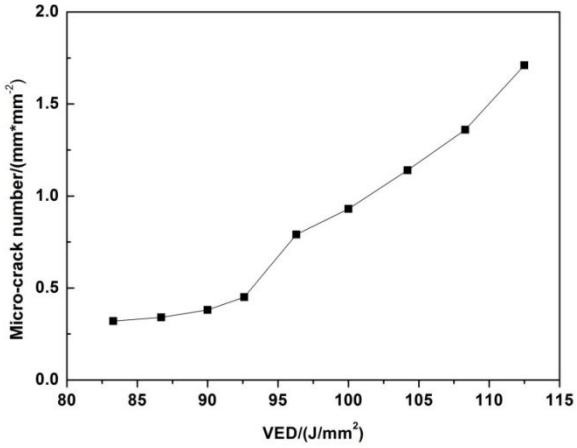


Figure 8. The effect of VED on the number of micro-cracks in the sample.

3.3.2 Effect of VED on density of SLM samples.

The density of SLM sample was measured by drainage method, divided by the density of GH3536 hot rolled bar as its density value.According to the table, the density of GH3536 alloy hot rolled bar is 8.3g/cm^3 [11]. Figure 9 shows the variation curve of the density of the SLMsample with VED increases. The existence of defects such as pores and micro-cracks in the sample will reduce the density of the sample. With the increase of VED, the density of SLM samples increases first and then decreases. When VED increases to 104.2J/mm^3, the density of the sample reaches the maximum value of 8.22g/cm^3.Compared with the density of hot rolled bars, the density is 99%. As VED continues to increase, the density of the sample decreases and stabilizes around 8.2g /cm^3.

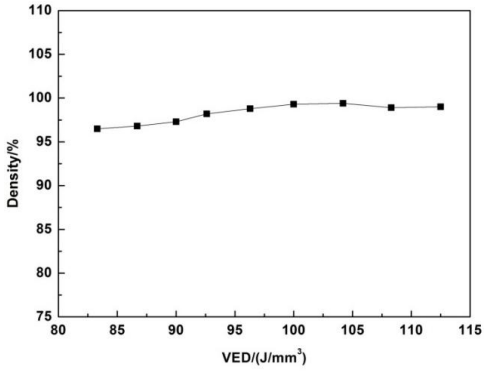


Figure 9. The effect of VED on density of the samples.

3.3.3Effect of VED on Vickers hardness of SLM samples.

Figure 10 is the variation curve of Vickers hardness of SLM samples with increase of VED. It can be seen from the diagram that with the increase of VED, the Vickers hardness of the sample gradually increases. When VED is 96.3J/mm^3, the Vickers hardness reaches 237 HV. With the continuous increase of VED, the Vickers hardness tends to be stable at about 242HV. Vickers hardness characterizes the ability of the material to resist local plastic deformation. When there are pores inside the sample, the pores collapse under the action of external pressure, which reduces the Vickers hardness value of the material. As the number of pores decreases, the Vickers hardness value gradually increases to maintain stability. The presence of micro-cracks has no significant effect on Vickers hardness.

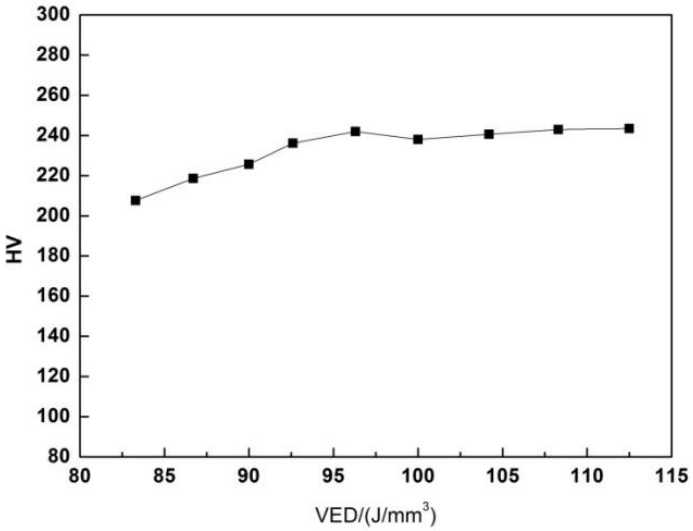


Figure 10. The effect of VED on Vickers hardness of the samples.

3.3.4 Effect of VED on mechanical properties of SLM samples.

Figure 11 shows the tensile curves of GH3536 samples with the increase of VED. It can be seen from the figure that GH3536 prepared by SLM method has a typical plastic deformation process and an obvious yield process. The tensile strength of the samples is between 740~780MPa.

Figure12 is the SEM photographs of the fracture of SLM samples. It can be seen from the figure that the fracture of the SLM samples shows typical dimple fracture char-acteristics, and obvious secondary intergranular cracks are formed. A large number of hard and brittle carbides are distributed on the grain boundary of SLM samples. During the tensile process, the carbides broke before the austenite matrix and generated micro-cracks. Under the action of stress, the cracks propagated along the grain boundary, and finally a fracture formed and secondary intergranular cracks generat-ed at the fracture. Due to the high plasticity of the austenite matrix, a large number of dimples were generated on the austenite matrix during the fracture process, and an intergranular dimple fracture was formed.

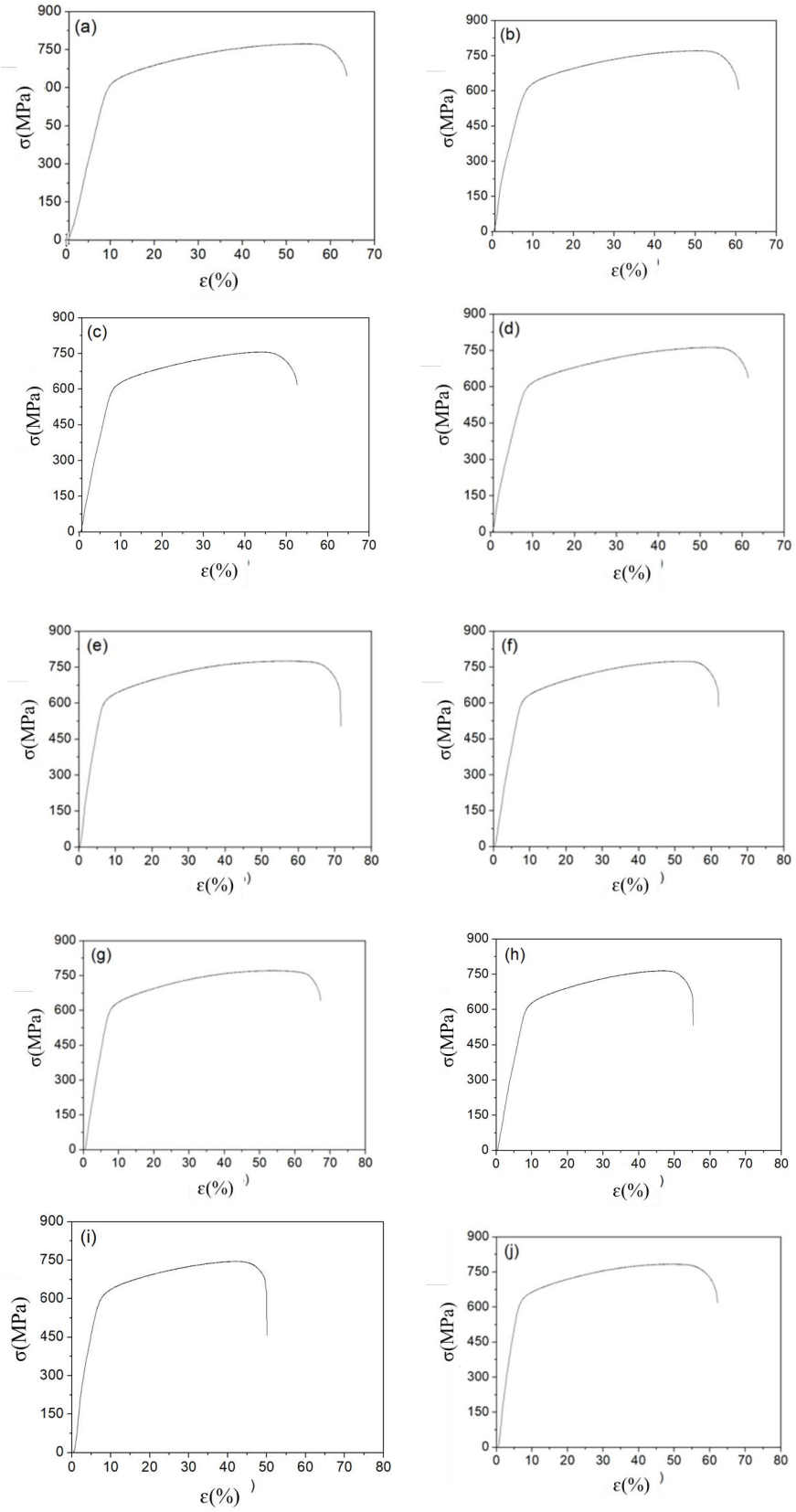


Figure 11. Tensile curves of GH3536 specimens prepared with different VED: (a) VED=83.3J/mm^3; (b) VED=86.7J/mm^3; (c) VED=90J/mm^3; (d) VED=92.6J/mm^3; (e) VED=96.3J/mm^3; (f) VED=100J/mm^3; (g) VED=104.2J/mm^3; (h)VED=108.3J/mm^3; (i) VED=112.5J/mm^3

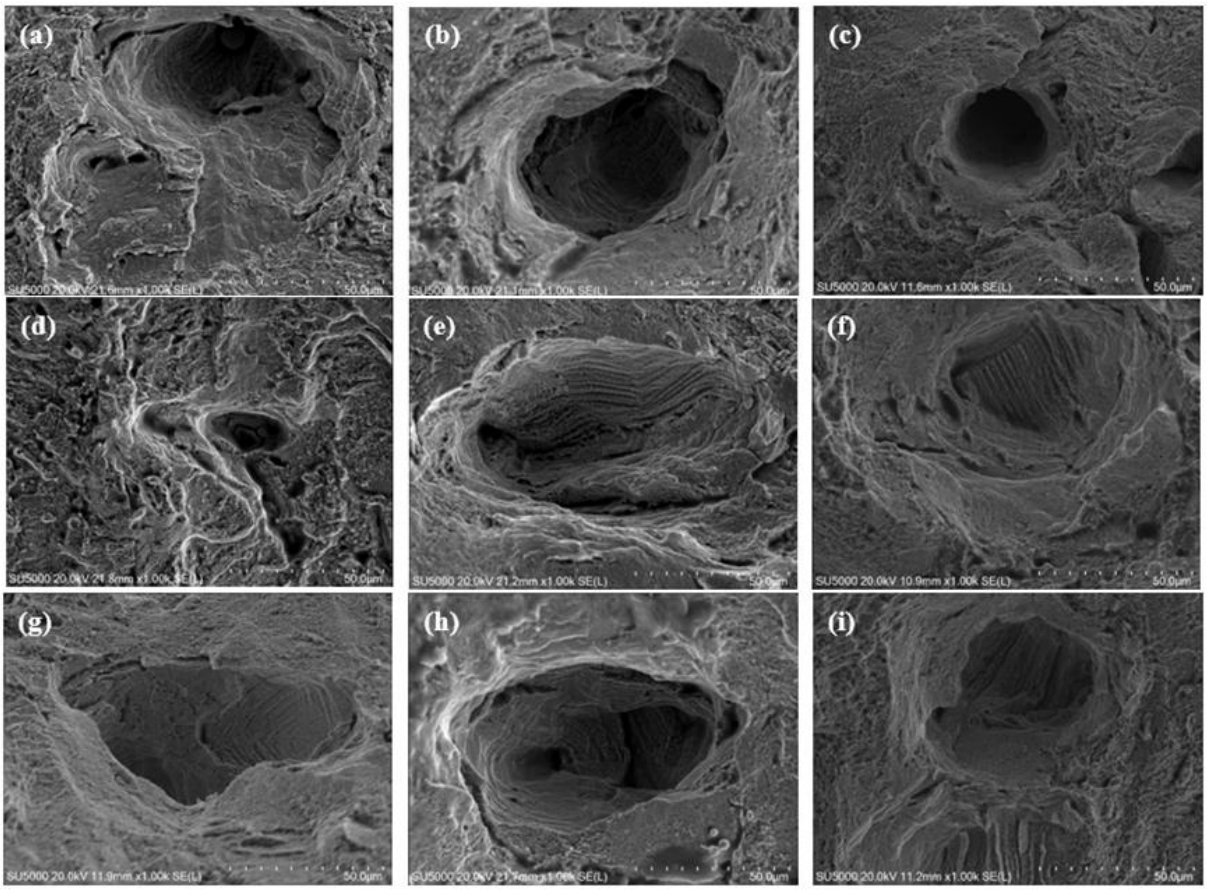


Figure 12. Tensile fracture of SLM samples with different VED: (a) VED=83.3J/mm^3; (b) VED=86.7J/mm^3; (c) VED=90J/mm^3; (d) VED=92.6J/mm^3; (e) VED=96.3J/mm^3; (f) VED=100J/mm^3; (g) VED=104.2J/mm^3; (h)VED=108.3J/mm^3; (i) VED=112.5J/mm^3

Figure13 is the effect of VED on the mechanical properties of SLM specimens. It can be seen from the figure that with the increase of VED, the tensile strength and yield strength of the material increase first and then decrease. The tensile strength is up to 772.3MPa and the yield strength is up to 613.3MPa, but the elongation of the mate-rial decreases at the same time.

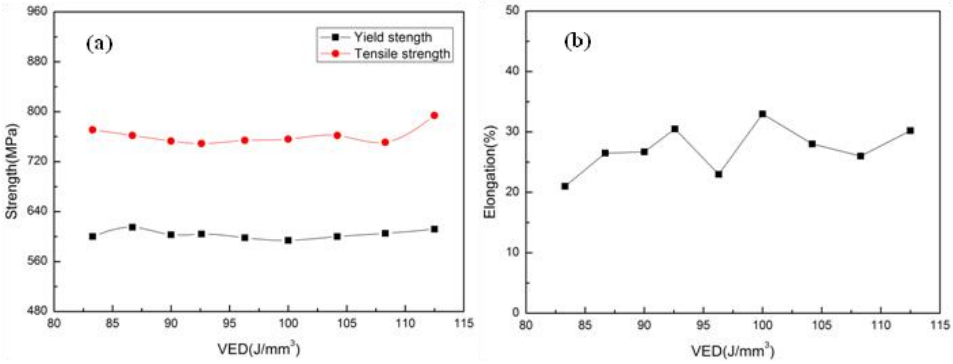


Figure 13. Effect of VED on the mechanical properties of SLM specimens.

3.4. Effect of heat treatment process on the mechanical properties of GH3536 samples

The tensile properties of GH3536 samples before and after heat treatment were tested at room temperature. The test results of tensile strength, yield strength, elongation and reduction of area are

shown in Table 4. Compared with SLM samples before heat treatment, it is found that the transverse and longitudinal tensile properties of the samples after heat treatment have higher tensile and yield strength at room temperatures, which are as high as 789MPa and 410MPa, respectively.

Table 4. Mechanical properties of GH3536 samples before and after heat treatment process

Sample	Direction	Tensile strength	Yield strength	Elongation	Section shrinkage rate
		MPa	MPa	%	%
SLM	transverse	721	336	33	44
	longitudinal	744	334	29	37
HT1	transverse	723	390	21	25
	longitudinal	784	401	19	17
HT2	transverse	735	398	17	20
	longitudinal	789	410	13	13

Compared with the SLM samples, the grain size of the sample after heat treatment is smaller, the number of grain boundaries is more, and the tensile strength is higher. When the carbides are distributed in blocks on the grain boundaries, the plasticity of the material will be seriously reduced. The grains of HT1 and HT2 samples are columnar crystals. In the longitudinal tensile process, most of the grain boundaries are parallel to the stress direction, and the effect on the plasticity is not obvious. In the transverse tensile process, the grain boundaries are perpendicular to the stress direction, which seriously reduces the plasticity of the sample. The grains of SLM samples are equiaxed grains, and the mechanical properties are not anisotropic. Because the grain boundary precipitates are continuously distributed in chains, the material has high plasticity.

Figure14 shows the SEM photographs of tensile fracture of GH3536 samples before and after heat treatment. It can be seen from the figure that there are many dimples on SLM samples, and obvious secondary intergranular cracks are existed. A large number of hard and brittle carbides are distributed on the grain boundary of SLM samples. During the tensile process, the carbides broke before the austenite matrix and generate micro-cracks. Under the action of stress, the micro-cracks propagated along the grain boundary, and finally formed a fracture and generated secondary intergranular cracks at the fracture. Due to the high plasticity of the austenite matrix, a large number of dimples were generated on the austenite during the fracture pro-cess, and an intergranular dimple fracture was formed. Compared with SLM samples, the number of dimples in HT1 and HT2 samples decreased significantly, and river patterns and cleavage planes appeared inside the materials, which indicated that the fracture mode of the sample has gradually transitioned from ductile fracture to intergranular cleavage fracture.

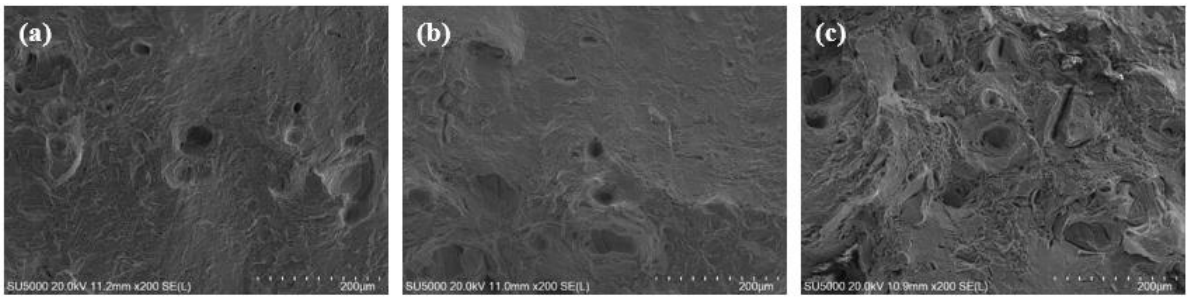


Figure 14. Effect of heat treatment on tensile fracture of GH3536 samples: (a) SLM; (b) HT1; (c) HT2

Through the analysis of the above mechanical properties, it can be seen that the SLM samples have good mechanical properties, whose performance index can reach the level of forgings. This is due to the multi-scale structure of the SLM samples, as shown in Figure15. In previous studies on 316

stainless steels, it was found that this cross-scale alloy structure greatly improved its mechanical properties and exceeded the superalloy prepared by traditional methods. The high cooling rate of the molten pool during the melting process of SLM samples significantly reduces the size ofmicrostructure and the range of composition segregation. At the same time, the composition segregation along the cell wall and the small-angle grain boundary can play a role in pinning dislocations, thereby improving material properties.

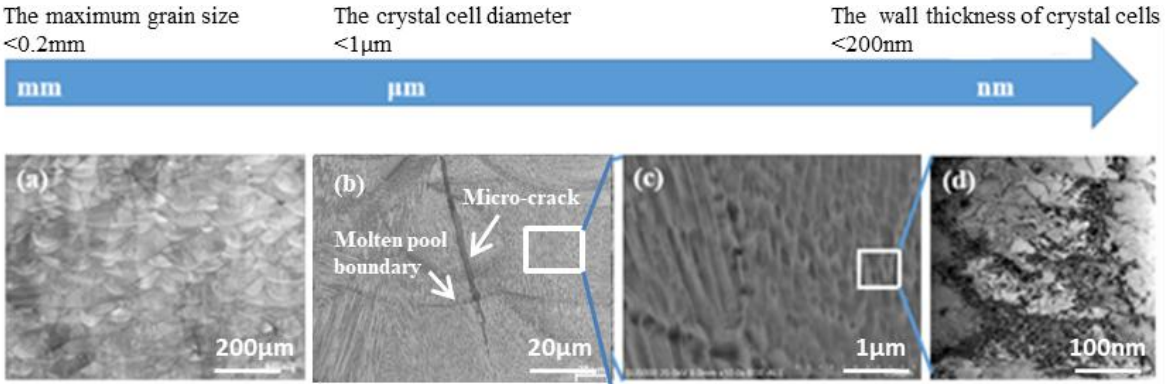


Figure 15. The multi-scale microstructure of GH3536 superalloy prepared by SLM.

4. Conclusions

(1) When VEDwas low, there were pores formed by unmelted powder between adjacent scanning lines of the same deposition layer and between adjacent deposition layers. With the increase of VED, the pores inside the samples gradually decreased and disappeared. When VED reached 96.3J/mm^3, micro-cracks began to appear inside the samples. The number of micro-cracks increased with the increase of VED. The size of micro-cracks in SLM sampleswas 10~100μm. The micro-cracks originated from the inside of the molten pool and penetrated the melting channel, which was due to the existence of Lavesphase at the grain boundary.

(2) Thedensity and Vickers hardness of SLM samples increased with the increase of VED, and gradually stabilized. The existence of pores reduced the density and Vickers hardness of the samples. However, the existence of micro-cracks had no obvious effect on the density and hardness.

(3) After heat treatment, the yield strength and tensile strength of the material were significantly improved, but the elongation was significantly reduced. The fracture mode of the sample gradually changed from ductile fracture to cleavage fracture.

5. References

[1] MaR,LiuL, WangY, BaiJ, TanC and SongX2022*Trans. China weld.Inst.***43** 73-79
[2] DingQ, BeiH and WeiX2021 *Mater.today nano***14**151-156
[3] LiA, LiuS and WangB 2018*J. ironsteel res. Int.***30**8-12
[4] Yang F, Hou J, Gao S, Wang C and Zhou L.*Mater. Sci.Eng. A.* 2018 **715**126-136
[5] BikasH,StavropoulosP and Chryssolouris G*Inter. J.Adv. Manuf. Tech.*2016**83**389-405
[6]Frazier W*J. Mater. Eng. Perform.*2014**23**1917-1928
[7]Wu,H, ChenF and LiuD*Mater. Sci.Forum* 2021**1035**152-160
[8] LiY, SongM and ZhangY*Mater. Sci.Forum* 2021 **1058**141-147
[9] Liu K*Physical Test. Chem. Anls* 2018**30**1866-1877
[10] XiaY, ChenH and LiangX*J. Manuf. Process.*2021**68**1694

Acknowledgments

This work was supported by Heilongjiang Provincial Institute Research Business Fee Project (Grant No. CZKYF2023-1-C039), and Talent Team Construction Platform Project of Heilongjiang Academy of Sciences (Grant No. RC2023GY01).